



Di-ruthenium complexes having diphosphines and carbonyls: Formation, structure, and catalytic hydrogenation of alkynes

Aparajita Mukherjee, Piyali Paul, Samaresh Bhattacharya*

Department of Chemistry, Inorganic Chemistry Section, Jadavpur University, Kolkata 700 032, India

ARTICLE INFO

Article history:

Received 15 November 2016

Received in revised form

28 December 2016

Accepted 30 January 2017

Available online 12 February 2017

Keywords:

Diphos and carbonyl ligands

Formation of di-ruthenium complexes

Catalytic hydrogenation of alkyne to alkene

ABSTRACT

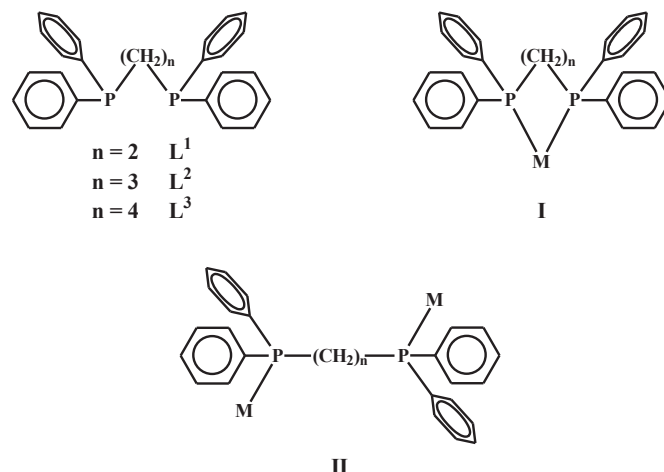
Reaction of three selected diphos ligands, viz. 1,2-bis(diphenylphosphino)ethane (L^1), 1,3-bis(diphenylphosphino)propane (L^2) and 1,4-bis(diphenylphosphino)butane (L^3), with $[Ru(CO)_2Cl_2]_n$ has afforded di-ruthenium complexes of type $[Ru_2(L)_3(CO)_2Cl_4]$, ($1-3$). Crystal structure of complex **1** has been determined, and molecular structures of complexes **2** and **3** have been optimized through DFT method. Formation of the unexpected di-ruthenium complexes has been probed through DFT calculations. In dichloromethane solution all the complexes show intense absorptions in the visible and ultraviolet regions. Cyclic voltammetry on the complexes shows an irreversible oxidation within 0.79–1.53 V vs SCE, and an irreversible reduction within -1.20 to -1.33 V vs SCE. The di-ruthenium complexes efficiently catalyze hydrogenation of alkynes to the corresponding alkenes.

© 2017 Elsevier B.V. All rights reserved.

1. Introduction

There has been considerable current attention to the chemistry of mixed-ligand ruthenium carbonyl complexes largely because of their versatile catalytic applications [1–16]. Reactivity of such complexes is dictated by the carbonyl and the ancillary ligands. Thus, binding of ligands of selected types to the metal center in the $Ru(CO)_n$ fragment is of significant importance for induction of desired properties in such mixed-ligand complexes. For the present study, which has originated from our interest in the chemistry of mixed-ligand ruthenium carbonyl complexes [17–21], we chose three diphos ligands ($L^1 - L^3$) with difference in separation between the two phosphorus donor sites. These phosphines were selected as ancillary ligands based on the fact that coordination of ruthenium by phosphines, in combination with the carbonyls, has often been found to be particularly useful for augmenting the catalytic activities of the resulting complexes [1–3,5–10,15]. The chosen diphos ligands are known to bind to a metal center usually as bidentate ligands forming stable chelate rings (**I**), but they are also known to serve as bridging ligands, where the two phosphorus sites remain linked with two metal centers (**II**) [22–25]. As the ruthenium starting material we selected $[Ru(CO)_2Cl_2]_n$, firstly because it contains a $Ru(CO)_2$ fragment in it, and secondly, and more importantly, because of its demonstrated ability to readily incorporate neutral chelating

bidentate ligands without dissociation of any pre-coordinated ligands [17,26–30]. Understandably, the primary aim was to obtain mixed carbonyl-phosphine-Ru complexes of type $[Ru(L)(CO)_2Cl_2]$ (L representing the diphos ligand) and explore their catalytic utility. Herein we describe our observations on the interaction of the selected diphos ligands with $[Ru(CO)_2Cl_2]_n$, with special reference to formation of new complexes, their structure and, their catalytic application in hydrogenation of alkynes.



* Corresponding author.

E-mail address: samaresh_b@hotmail.com (S. Bhattacharya).

2. Results and discussion

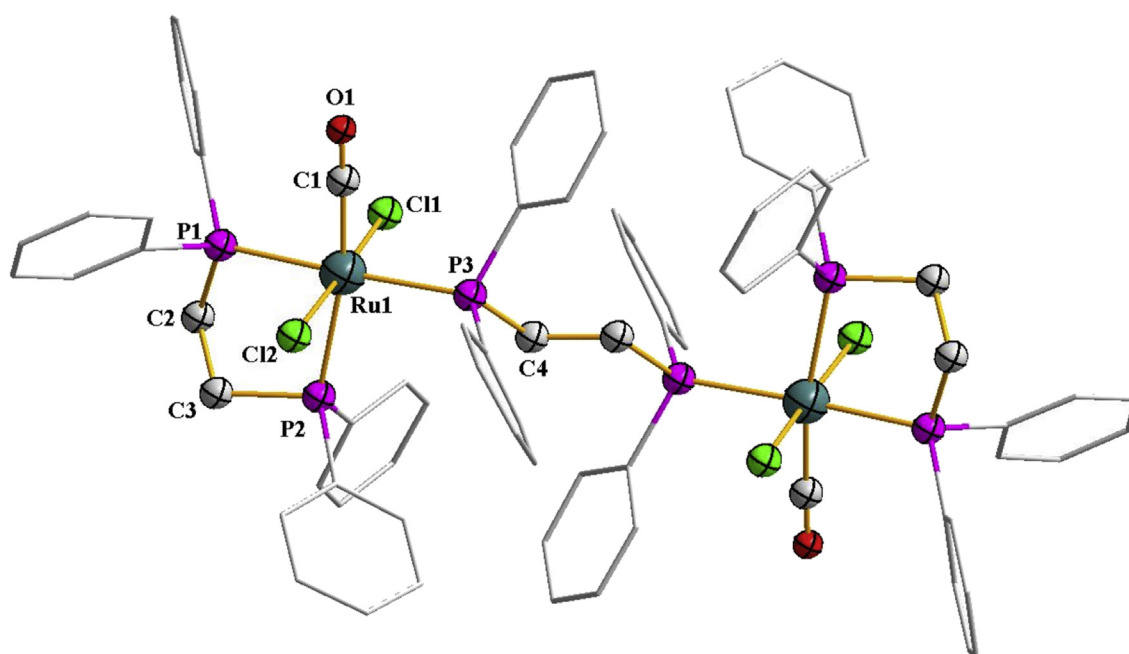
2.1. Synthesis and characterization

As outlined in the introduction, the primary goal of this study was to explore the interaction of the selected diphos ligands ($L^1 - L^3$) with $[Ru(CO)_2Cl_2]_n$ with an expectation of getting mixed-ligand complexes of type $[Ru(L)(CO)_2Cl_2]$. Accordingly a reaction of $[Ru(CO)_2Cl_2]_n$ was first carried out with L^1 in equimolar ratio, where the mole calculation of the ruthenium precursor was done based on the $Ru(CO)_2Cl_2$ unit. The reaction proceeded smoothly in refluxing methanol to afford a yellow complex in rather poor yield. The yield improved on increasing Ru: L^1 ratio to 1:1.5, which is described in the experimental section. Characterization on the complex (*vide infra*) showed it to have a significantly different composition, viz. $[Ru_2(L^1)_3(CO)_2Cl_4]$, (**1**), than what was expected. The low yield is attributable to unavailability of adequate quantity of the diphos ligand (L^1), required with respect to the Ru-starting material, for the formation of this di-ruthenium complex. This was further demonstrated by carrying out a similar reaction with 1.5 equivalents of L^1 , which afforded the same complex **1** in much better yield. Similar results were observed for reactions of $[Ru(CO)_2Cl_2]_n$ with the other two diphos ligands, viz. L^2 and L^3 , both of which yielded di-ruthenium complexes of the same type, viz. $[Ru_2(L^2)_3(CO)_2Cl_4]$, (**2**) and $[Ru_2(L^3)_3(CO)_2Cl_4]$, (**3**), respectively. Preliminary characterizations (microanalysis, mass, NMR and IR) of the isolated products agree well with their compositions. Mass spectrum of each di-ruthenium complex (general formula $[Ru_2(L)_3(CO)_2Cl_4]$) shows three characteristic peaks, one corresponding to the $[Ru_2(L)_3(CO)_2Cl_3]^+$ ion, and the other two peaks indicate that, under the mass spectral condition, the di-ruthenium complexes (**1**, **2** and **3**) have undergone rapid fragmentation into two parts (**1a**, **1b**; **2a**, **2b**; and **3a**, **3b**) having general composition $Ru(L)_2(CO)Cl_2$ and $Ru(L)(CO)Cl_2$, respectively. In order to identify the bridging ligand in these di-ruthenium complexes, as well as to find out coordination mode of the diphos ligands in them, structure of complex **1** was determined by X-ray crystallography. The

Table 1
Selected bond lengths (Å) and bond angles (°) for complex **1**.

Bond lengths (Å)			
Ru1-Cl1	2.4221(11)	C1-O1	1.076(6)
Ru1-Cl2	2.4001(11)	P1-C2	1.810(4)
Ru1-P1	2.3580(10)	C2-C3	1.524(6)
Ru1-P2	2.4937(11)	P2-C3	1.844(4)
Ru1-P3	2.3980(9)		
Ru1-C1	1.882(5)		
Bond angles (°)			
Cl1-Ru1-Cl2	175.75(4)	P1-Ru1-P2	82.95(4)
P1-Ru1-P3	176.73(4)	Ru1-C1-O1	177.4(5)
P2-Ru1-C1	169.63(14)		

structure is shown in Fig. 1, and selected bond parameters are listed in Table 1. The structure shows that out of the three diphos ligands present in the complex molecule, two are coordinated, separately, to the two ruthenium centers forming five-membered chelate rings (**I**, $n = 2$, $M = Ru$), while the third diphos ligand is coordinated to both the ruthenium centers in a bridging mode (**II**, $n = 2$, $M = Ru$). Two chlorides and a carbonyl are coordinated to each ruthenium center. The chelated diphos ligand, the carbonyl and the phosphorus of the bridging diphos ligand constitute an equatorial plane around each ruthenium, and the two chlorides occupy mutually *trans* positions. The Ru-P bond, that is *trans* to the coordinated carbonyl, is found to be significantly longer than the other two Ru-P bonds. The remaining bond distances around ruthenium are all found to be quite usual [17–21]. The other two di-ruthenium complexes (**2** and **3**), which were synthesized similarly and show similar properties (*vide infra*), are assumed to have similar structures as complex **1**. As crystals of complexes **2** and **3** could not be grown, their expected structures were optimized with the help of Density Functional Theory (DFT) method [31]. The optimized structures are shown in Fig. 2 and Fig. 3, and some computed bond parameters are given in Table S1 (Supplementary material). For a proper comparison of bond parameters in the DFT-optimized



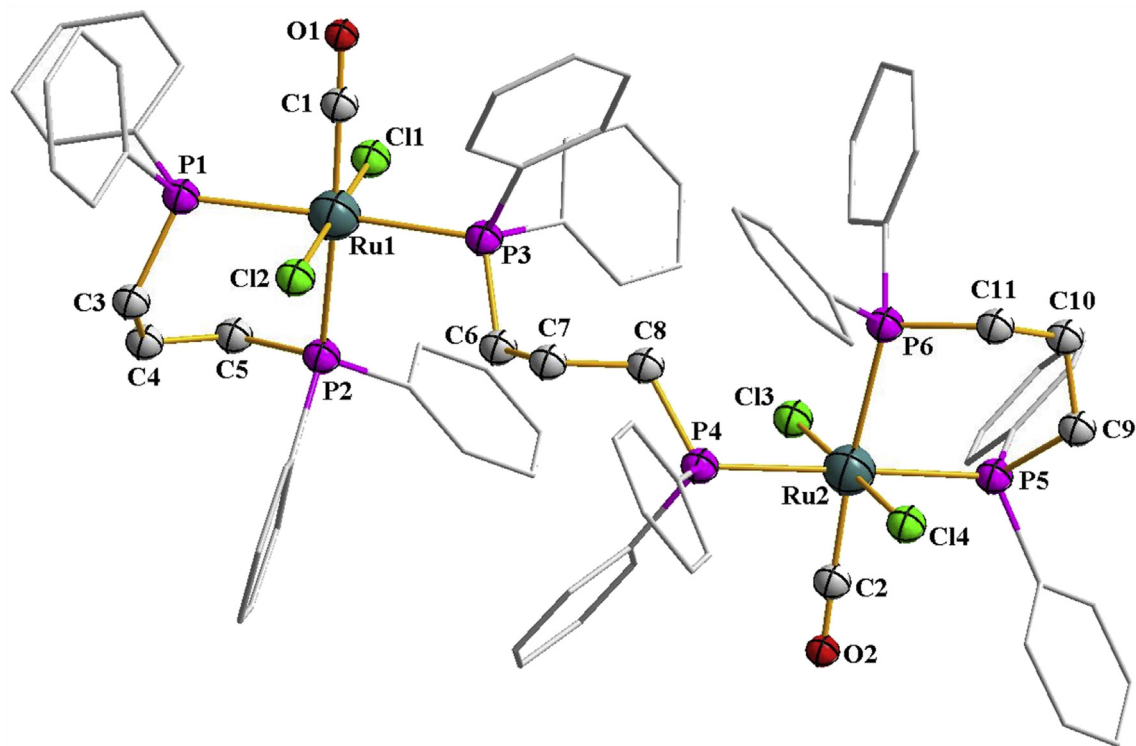


Fig. 2. DFT-optimized structure of complex 2.

structures, structure of complex 1 was also optimized by DFT method, which is shown in Fig. S1 (Supplementary material) and some computed bond parameters are included in Table S1. The DFT-optimized structure of complex 1 and the associated bond parameters are found to compare well with its crystal structure and bond parameters obtained thereby. In the other two complexes, 2 and 3, the core structure around each ruthenium center is found to

be qualitatively similar to that in complex 1. The computed bond parameters of the DFT-optimized structures of all the three complexes are found to be very much comparable (Table S1). However, the Ru-Ru distance is found to increase expectedly with increasing number of CH₂ fragment in the bridging diphos ligand. Similarly, in the Ru(P-P) chelate, P-P depicting the chelated diphos ligand, size of the chelate ring and the P-Ru-P bond angle are also found to

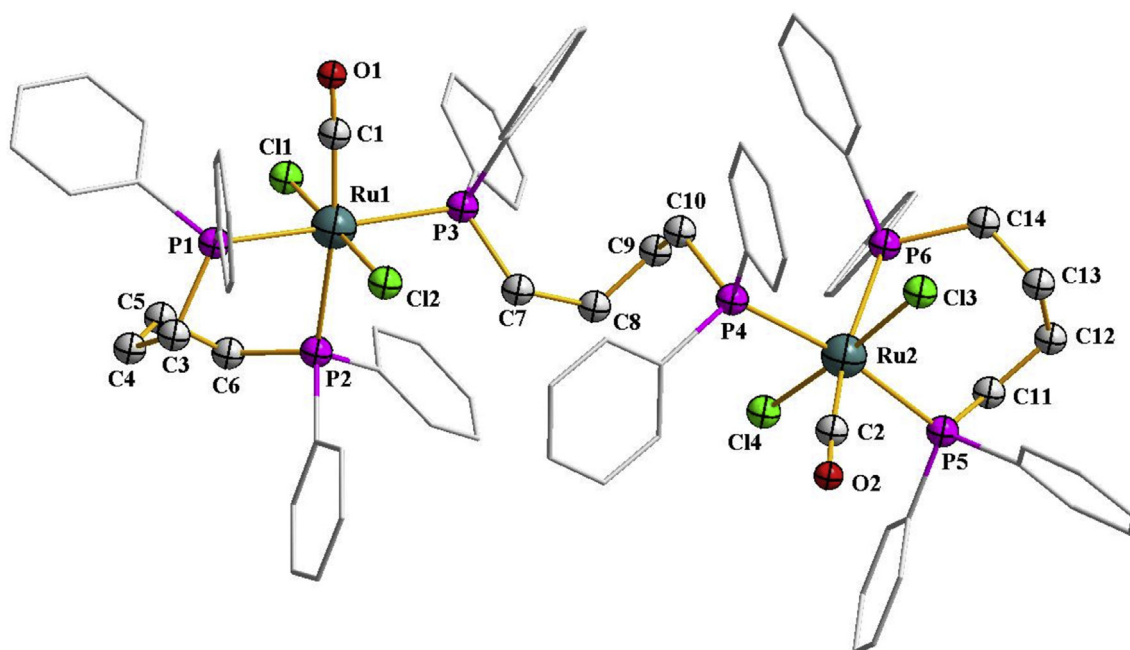
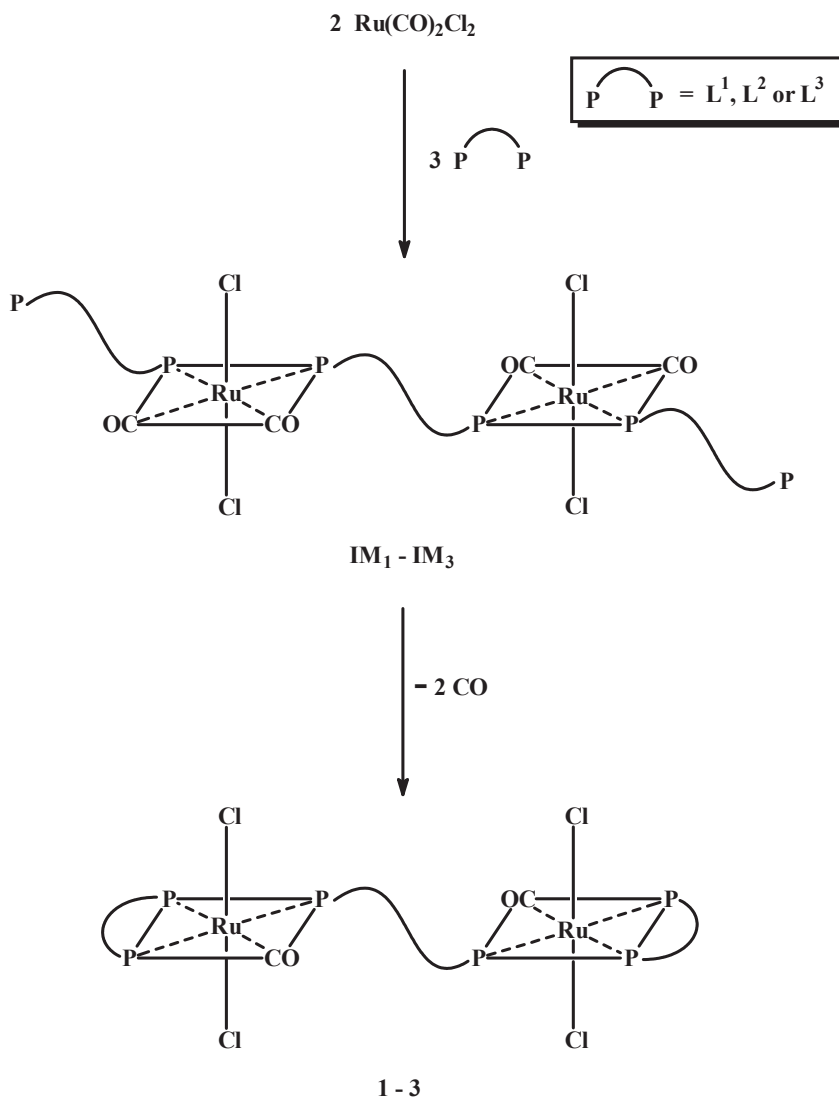


Fig. 3. DFT-optimized structure of complex 3.



Scheme 1. Probable steps behind formation of the di-ruthenium complexes **1** - **3**.

increase with increasing number of CH_2 fragment between the two phosphorus donors.

Formation of the di-ruthenium complexes of type $[\text{Ru}_2(\text{L})_3(\text{CO})_2\text{Cl}_4]$, instead of the expected mixed-ligand complexes of type $[\text{Ru}(\text{L})(\text{CO})_2\text{Cl}_2]$, even from reactions between equimolar amounts of the diphos ligand and $\{[\text{Ru}(\text{CO})_2\text{Cl}_2]_n\}$, has been quite intriguing. In view of the fact that the three chosen diphos ligands remain in an unfolded chain form in their native states [32–34], we have invoked a set of plausible sequences behind formation of the di-ruthenium complexes, which are illustrated in Scheme 1.

Herein, we speculate that the diphos ligands initially bind to the coordinatively unsaturated metal center in the $\text{Ru}(\text{CO})_2\text{Cl}_2$ unit, retaining their native unfolded geometry, forming a di-ruthenium species as intermediate ($\text{IM}_1 - \text{IM}_3$). In the next step, the two terminal diphos ligands fold around the metal centers and thereby the so far uncoordinated phosphorus atoms bind to the metal centers, via dissociation of a carbonyl from each ruthenium, forming two $\text{Ru}(\text{P}-\text{P})$ chelate rings, and thus affording the di-ruthenium complexes **1**–**3**.

The thermodynamics for the formation of complex **1** was investigated computationally by DFT. The reactive $\text{Ru}(\text{CO})_2\text{Cl}_2$ fragment in the starting ruthenium complex, and the diphos ligand

L^1 were optimized by DFT, as were the remaining species depicted in Scheme 1. Stable geometries, having only positive eigenvalues, were found for each species, and this allowed us to determine the thermodynamics for the observed transformation that affords complex **1**. The optimized structures and ground-state energy ordering for the pertinent species are depicted in Fig. 4. The $\text{Ru}(\text{CO})_2\text{Cl}_2$ unit (**A**) has a tetrahedral geometry and the uncoordinated 1,2-bis(diphenylphosphino)ethane (**B**) has the unfolded chain structure. The reaction of **A** and **B** gives the di-ruthenium intermediate species (**C**), in which both terminal and bridging diphos ligands are having similar unfolded geometry as the uncoordinated diphos ligand (**B**). Formation of **C** is exergonic and the reaction lies 111.2 kcal/mol below the reagents. Species **C** is converted to the final di-ruthenium complex **1** (**D**) via elimination of CO (**E**). The $\text{C} \rightarrow \text{D} + 2 \text{ E}$ reaction is also exergonic and lies 2.5 kcal/mol below the intermediate **C**. The net thermodynamics are computed at -113.7 kcal/mol and are in agreement with the easily prepared and readily isolable nature of the di-ruthenium complexes.

We also considered an alternative mechanism behind formation of the di-ruthenium complexes, which was also believed to proceed in a step-wise fashion, as illustrated in Scheme S1 (Supplementary

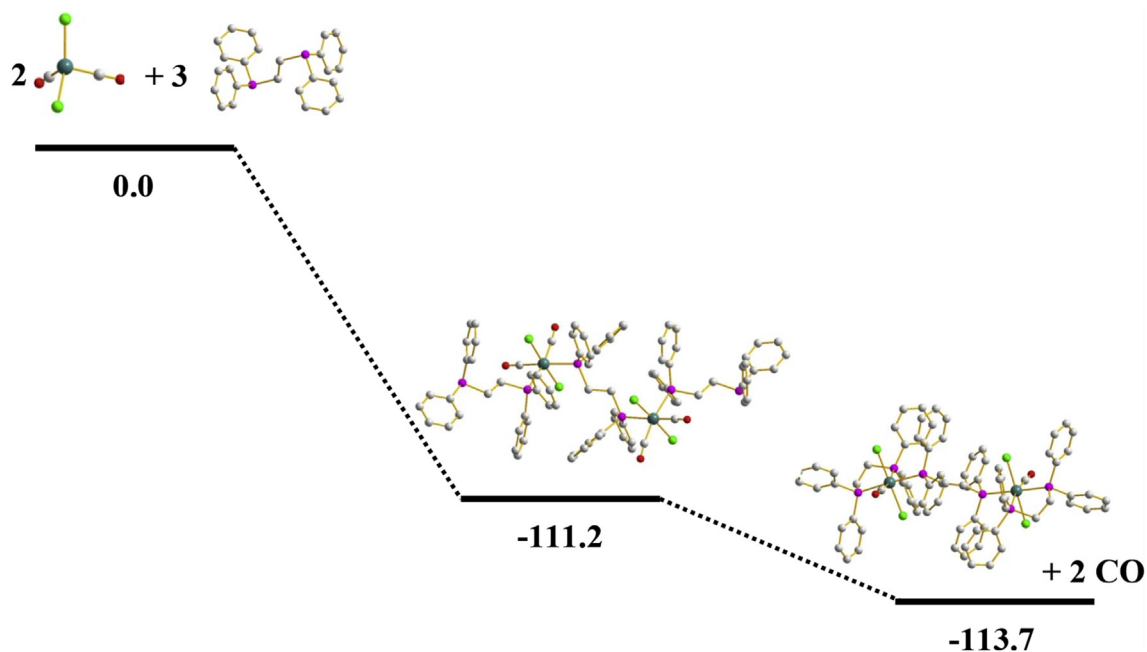


Fig. 4. DFT-optimized structures and ground-state energy ordering for the reaction of $\text{Ru}(\text{CO})_2\text{Cl}_2$ (**A**) and 1,2-bis(diphenylphosphino)ethane (**B**) to give the di-ruthenium complex $[\text{Ru}_2(\text{L}^1)_3(\text{CO})_2\text{Cl}_4]$ (**D**) and CO (**E**), via formation of $[\text{Ru}_2(\text{L}^1)_3(\text{CO})_4\text{Cl}_4]$ (**C**). The free energy values (in kcal/mol) are referenced relative to the reagents ($2\text{A}+3\text{B}$). The optimized structure for **E** is not shown.

material). In the first step, the diphos ligand binds, in the chelating mode, to the coordinatively unsaturated ruthenium center in the $\text{Ru}(\text{CO})_2\text{Cl}_2$ unit, yielding a complex of type $[\text{Ru}(\text{L})(\text{CO})_2\text{Cl}_2]$ as an intermediate ($\text{X}_1 - \text{X}_3$). In the next step, one of the two carbonyls in this intermediate undergoes facile displacement by a phosphorus at one end of a second diphos ligand, while the phosphorus at the other end of the same diphos ligand links itself to a second ruthenium center via similar displacement of a carbonyl, and thereby affords the di-ruthenium complexes. The thermodynamics for this alternative mechanism was also investigated by DFT for complex **1**, and all the species involved in its formation, as depicted in Scheme S1, were optimized. The optimized structures and ground-state energy ordering for all the relevant species are shown in Fig. S2 (Supplementary material). Initial reaction of $\text{Ru}(\text{CO})_2\text{Cl}_2$ (**A**) and 1,2-bis(diphenylphosphino)ethane (**B**) gives the intermediate (**C**), in which the diphos ligand is chelated to ruthenium. Formation of **C** is exergonic and the reaction lies 62.9 kcal/mol below the reagents. Species **C** further reacts with the diphos ligand (**B**) and is converted to the di-ruthenium complex **1** (**D**) via elimination of CO (**E**). The $\text{C} + \frac{1}{2}\text{B} \rightarrow \frac{1}{2}\text{D} + \text{E}$ step is found to be endergonic by 6.0 kcal/mol, and hence it is thermodynamically unfavorable. Thus we are inclined to believe that formation of the di-ruthenium complexes proceeds through the two steps shown in Scheme 1, where both the steps are thermodynamically favorable.

2.2. Spectral studies

Magnetic susceptibility measurements show that all the three di-ruthenium complexes are diamagnetic, which corresponds to the +2 oxidation state of ruthenium (low-spin d^6 , $S = 0$) in them. ^1H NMR spectra of the complexes show broad signals within 6.5–8.2 ppm due to overlapping phenyl-proton signals arising from twelve phenyl rings from three coordinated diphos ligands in each complex molecule. The methylene-proton signals, arising from six, nine or twelve $-\text{CH}_2-$ fragments in the three complexes, also appear as overlapping signals within 2.2–3.0 ppm, and hence no clear P-H coupling was visible. ^{31}P NMR spectrum of each complex shows

three distinct signals, each as a triplet due to coupling with the two proximal methylene protons, consistent with the nonequivalent nature of the three phosphorous nuclei in each half of the di-ruthenium complex. Infrared spectra of the complexes show many bands of varying intensities within $4000 - 450 \text{ cm}^{-1}$. While a detailed spectral assignment has not been attempted due to the complex nature of the spectra, a strong $\nu(\text{CO})$ stretch could be easily identified within $1960 - 1965 \text{ cm}^{-1}$. The remaining bands within $489 - 1638 \text{ cm}^{-1}$ are attributable to the coordinated diphos ligands [35]. Besides, two distinct bands near 2920 and 3054 cm^{-1} are due to methylenic C-H and phenyl C-H stretches respectively.

The di-ruthenium complexes were found to be readily soluble in dichloromethane and chloroform, producing light yellow solutions. Electronic spectra of the complexes were recorded in dichloromethane solutions, and the spectral data are given in Table 2. Each complex shows an absorption of moderate intensity around 370 nm, and few intense absorptions at shorter wavelengths. In order to gain some idea about the nature of the lowest energy absorption, we examined the character of the HOMO and LUMO of these complexes. Contour plots of these two orbitals for complex **1** are shown in Fig. 5, and those for the other two complexes are presented in Fig. S3 and Fig. S4 (Supplementary material). Composition of the HOMO and LUMO of all the complexes is given in Table 3. In complex **1** the HOMO is found to be delocalized

Table 2
Electronic spectral and cyclic voltammetric data.

Complex	Electronic spectral data ^a λ_{max} , nm (ϵ , $\text{M}^{-1} \text{ cm}^{-1}$)	Cyclic voltammetric data ^b E/V vs. SCE
1	371 ^c (700), 269 (39500)	0.79 ^d , -1.33 ^e
2	370 ^c (900), 271 ^c (50400), 249 ^c (62500)	1.16 ^d , -1.20 ^e
3	371 ^c (1300), 272 ^c (38500), 250 ^c (60000)	1.53 ^d , -1.26 ^e

^a In dichloromethane.

^b Solvent, dichloromethane; supporting electrolyte, TBHP; scan rate, 50 mVs^{-1} .

^c Shoulder.

^d E_{pa} value.

^e E_{pc} value.

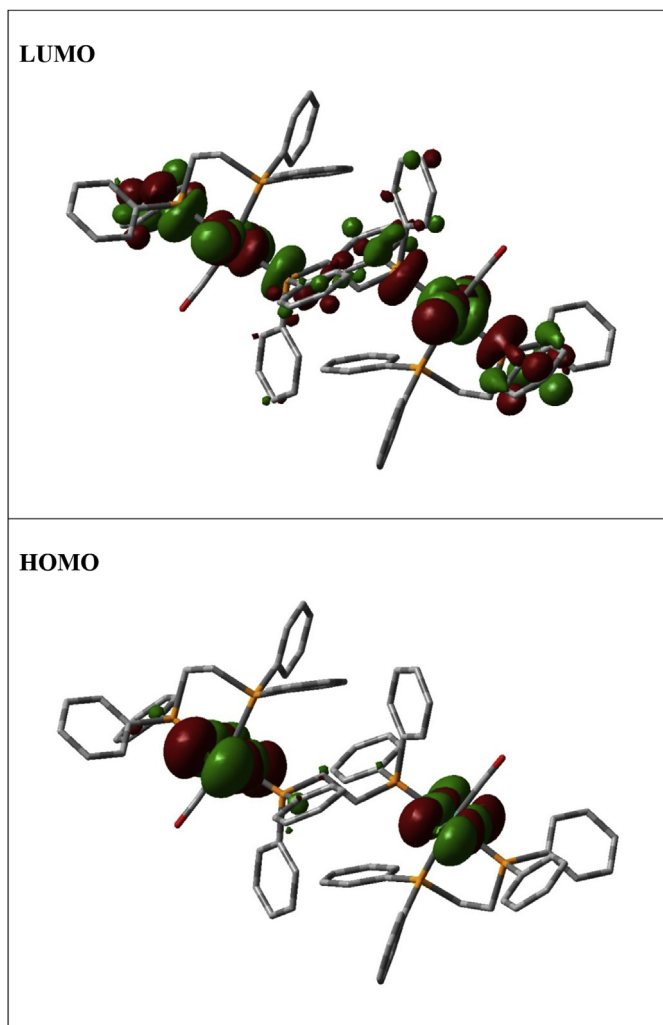


Fig. 5. Contour plots of the HOMO and LUMO of complex 1.

primarily (69%) over the two metal centers, with much less (27%) contribution from the coordinated chlorides, while the LUMO is distributed over the two metal centers (~27%), the chlorides (~24%), the two chelated diphos ligands (~22%) and the bridging diphos ligand (~27%). The lowest energy absorption in complex **1** is hence assignable to a transition from a filled orbital having mixed (metal + chloride) character to a vacant orbital also having mixed (metal + chloride + diphos) character. In complexes **2** and **3**, though distribution of HOMO and LUMO over the different fragments is different than that in complex **1** (Table 3; Fig. S3 and Fig. S4), the overall nature of the lowest energy transition is found to be qualitatively similar to that in complex **1**.

2.3. Electrochemical properties

Redox activity of the di-ruthenium complexes was examined in dichloromethane solution (0.1 M TBHP) by cyclic voltammetry. Voltammetric data are presented in Table 2. Each complex shows an irreversible oxidation within 0.7–1.6 V and an irreversible reduction within –1.2 to –1.4 V (all potentials are referenced to saturated calomel electrode (SCE)), which are tentatively assigned to Ru(II)–Ru(III) oxidation and reduction of the diphos ligand. Appearance of a single oxidative response for these di-ruthenium complexes, where the two metal centers are having identical coordination

Table 3
Composition of selected molecular orbitals of the complexes.

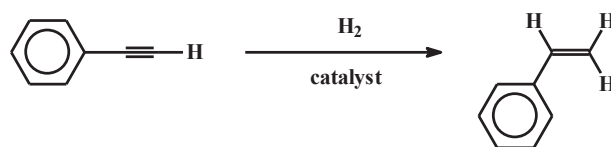
Complex	Contributing fragments	% Contribution of fragments to		
		HOMO	LUMO	
1	Ru(L ¹)(CO)Cl ₂	Ru1	35.3	13.3
		Cl1 + Cl2	13.6	10.3
	CO	0.0	0.0	
	L ¹	1.3	10.8	
	bridging L ¹ Ru(L ¹)(CO)Cl ₂	Ru2	2.7	26.7
		Cl3 + Cl4	33.7	14.0
		CO	13.4	13.6
L ¹		0.0	0.0	
2	Ru(L ²)(CO)Cl ₂	Ru1	46.6	1.4
		Cl1 + Cl2	32.9	0.0
	CO	0.0	0.0	
	L ²	9.8	0.0	
	bridging L ² Ru(L ²)(CO)Cl ₂	Ru2	10.7	24.1
		Cl1 + Cl2	0.0	26.3
		CO	0.0	18.5
L ²		0.0	0.0	
3	Ru(L ³)(CO)Cl ₂	Ru1	45.7	21.3
		Cl1 + Cl2	36.1	19.6
	CO	0.0	0.7	
	L ³	8.0	10.2	
	bridging L ³ Ru(L ³)(CO)Cl ₂	Ru2	10.2	26.4
		Cl1 + Cl2	0.0	11.0
		CO	0.0	10.5
L ³		0.0	0.0	

environments, indicates that there is no observable communication between the two metal centers.

2.4. Catalysis

As already mentioned in the introduction that ruthenium complexes having carbonyl and phosphine in the coordination sphere are finding wide application as catalysts in a variety of organic transformations, we were keen to find catalytic utility of the present group of complexes. And encouraged by some recent studies on the utilization of such complexes as catalyst for the hydrogenation of alkynes to alkenes [36–43], we planned to explore similar reactions using our di-ruthenium complexes as catalyst. We began our study by examining the hydrogenation of phenylacetylene using gaseous hydrogen at 1 atm and complex **1** as catalyst to furnish the corresponding hydrogenated product, viz. styrene. Table 4 provides information on the impact of various reaction parameters on the efficiency of this process. After extensive optimization, we found that 2.0 mol% catalyst, toluene as solvent, 110° C reaction temperature, and 10 h reaction time, furnish the desired alkene in good (65%) yield (entry 1), and no alkane is produced in the reaction. As expected, in the absence of the ruthenium catalyst, no hydrogenation occurs (entry 2). Decrease in the catalyst loading, relative to the optimum value, results in significant decrease in the yield (entry 3), while increase in the catalyst loading leads to only insignificant improvement in the yield (entry 4). Upon reducing the reaction time, the yield is found to decrease significantly (entry 5). However, upon increasing the reaction time, to twice the optimum value, results only in slight increase in the yield (entry 6). Lowering the reaction temperature, relative to the optimum value, causes decrease in the yield (entry 7). Among the solvents tried, toluene turned out to be the most suitable. For example, no hydrogenation is observed to take place

Table 4
Optimization of experimental parameters.^a



Entry	Solvent	Catalyst	Mole % of catalyst	Temperature, °C	Time, h	Yield ^b , %
1	toluene	1	2.0	110	10	65
2	toluene	–	–	110	10	NO ^c
3	toluene	1	1.5	110	10	44
4	toluene	1	3.0	110	10	71
5	toluene	1	2.0	110	8	47
6	toluene	1	2.0	110	20	69
7	toluene	1	2.0	70	10	45
8	chloroform	1	2.0	60	10	NO ^c
9	acetonitrile	1	2.0	80	10	NO ^c
10	toluene	2	2.0	110	10	67
11	toluene	3	2.0	110	10	64

^a Reaction conditions: phenylacetylene (0.5 mmol), H₂ gas (1.0 atm), solvent (5.0 mL).

^b Determined by GCMS.

^c Not observed.

upon changing the solvent to chloroform or acetonitrile (entries 8 and 9). Under the optimized condition, the other two di-ruthenium complexes also show similar catalytic efficiency as complex **1** (entries 10 and 11).

The scope of the reaction is shown in Table 5. As all the di-ruthenium complexes have shown comparable catalytic efficiency, only the results obtained with complex **1** as the catalyst are highlighted here. Using the optimized the reaction conditions, hydrogenation reactions have been performed on a series of ten different alkynes. Using phenylacetylene and substituted phenylacetylenes as substrates (**S**₁ – **S**₇), the corresponding alkenes (**P**₁ – **P**₇) were obtained in good (64–72%) yields. Both electron-withdrawing and electron-donating substituents were used, but the yields remained rather indifferent to the nature of the substituents. While alkynes with both R₁ ≠ H and R₂ ≠ H, viz. 1-phenyl-1-propyne, diphenylacetylene and bis(4-pyridyl)acetylene, were used as substrates (**S**₈ – **S**₁₀), the corresponding alkenes were obtained in both *cis* (**P**_{8a} – **P**_{10a}) and *trans* (**P**_{8b} – **P**_{10b}) forms. However, yield of the *cis*-alkene (6–10%) was always found to be much less than that of the *trans*-alkene (52–63%), which is usually observed as well as expected from steric consideration. All the product alkenes were isolated and characterized by ¹H NMR studies. Separation of *cis* and *trans* isomers of the last three alkenes (**P**₈ – **P**₁₀) has not been possible, however, NMR spectra recorded on the mixture of two isomers clearly indicated the presence of *trans*-isomer in considerable excess over the *cis*-isomer. It is noteworthy that further reduction of alkene to alkane has not been encountered in any of these attempted hydrogenation reactions. The catalytic efficiency of the present group of complexes is found to be comparable to that of some other ruthenium complexes reported recently [37,39,40,42].

The observed catalytic hydrogenation of alkynes is believed to follow sequences, illustrated in Scheme 2, that are essentially drawn from those proposed earlier [36,38,42]. In the di-ruthenium catalyst-precursor, each ruthenium has identical P₃Cl₂(CO) coordination environment, which is depicted as (**i**). Dissociation of a Ru-P bond, which may be from the chelated diphos or from the bridging diphos ligand, is believed to take place initially, producing a 16e species (**ii**), and thus enabling the alkyne to bind to the metal center in a π-fashion (**iii**). Which, in turn, triggers dissociation of a

carbonyl generating another 16e species (**iv**), and the catalytic cycle starts therefrom. The possibility of dissociation of CO first followed by that of the Ru-P bond, however, cannot be ruled out. Activation of molecular hydrogen takes place, initially via σ-interaction (**v**), eventually generating a dihydrido species (**vi**). Hydride transfer generates the Ru-C bonded species (**vii**). Reductive elimination of the alkene takes place, producing a ruthenium(II) species (**viii**) having P₂Cl₂ coordination sphere, and such four-coordinated ruthenium(II) species are well precedent in the literature [44–47]. This coordinatively unsaturated species immediately takes up an alkyne to regenerate the first member (**iv**) of the catalytic cycle, and thus it continues.

3. Conclusions

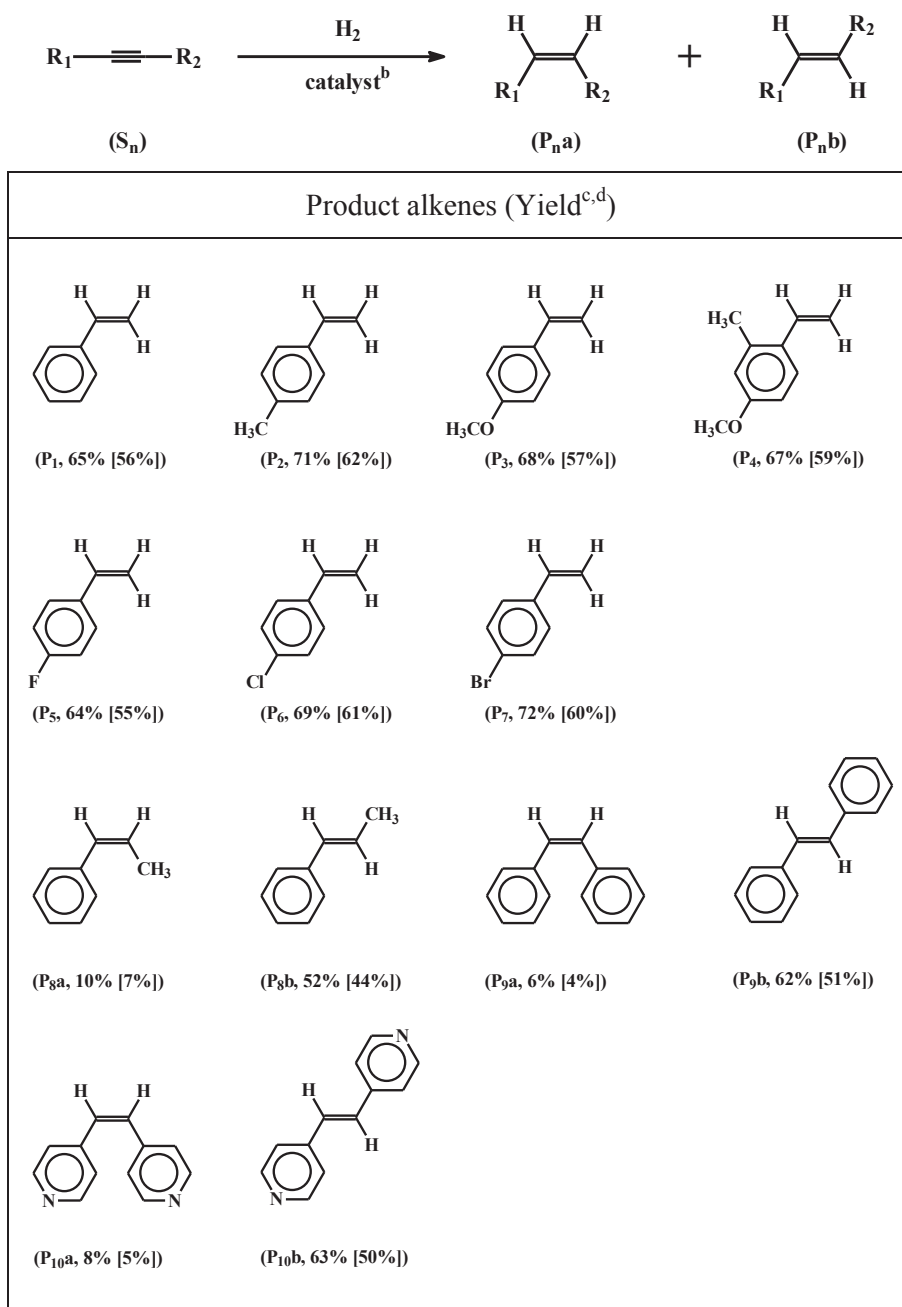
The present study shows that the diphos ligands (**L**¹ – **L**³), which remain in the unfolded chain form in their native state, readily interact with the metal center in the Ru(CO)₂Cl₂ fragment, provided by [{Ru(CO)₂Cl₂]_n, to afford di-ruthenium complexes of type [Ru₂(L)₃(CO)₂Cl₄] (**1**–**3**), where the diphos ligands display both chelating, as well as bridging, mode of binding. The di-ruthenium complexes can efficiently catalyze hydrogenation of alkynes, under relatively mild condition, to afford the corresponding alkenes. Dissociability of the Ru-CO and Ru-P bonds seems to play key roles behind the observed catalysis.

4. Experimental

4.1. Materials

Ruthenium trichloride was purchased from Arora Matthey, Kolkata, India. The diphos ligands (**L**¹ – **L**³) were procured from Aldrich. [{Ru(CO)₂Cl₂]_n was prepared by following a reported procedure [48]. Tetrabutylammonium hexafluorophosphate (TBHP), obtained from Aldrich, and AR grade acetonitrile, procured from Merck, India, were used for electrochemical work. All other chemicals and solvents were reagent grade commercial materials and were used as received.

Table 5
Hydrogenation of alkynes.^{a,b,c,d}



^a Reaction conditions: alkyne (0.5 mmol), H₂ gas (1.0 atm), toluene (5.0 mL), reaction temperature (110 °C), reaction time (10 h).

^b Catalyst: complex **1** (2.0 mol%).

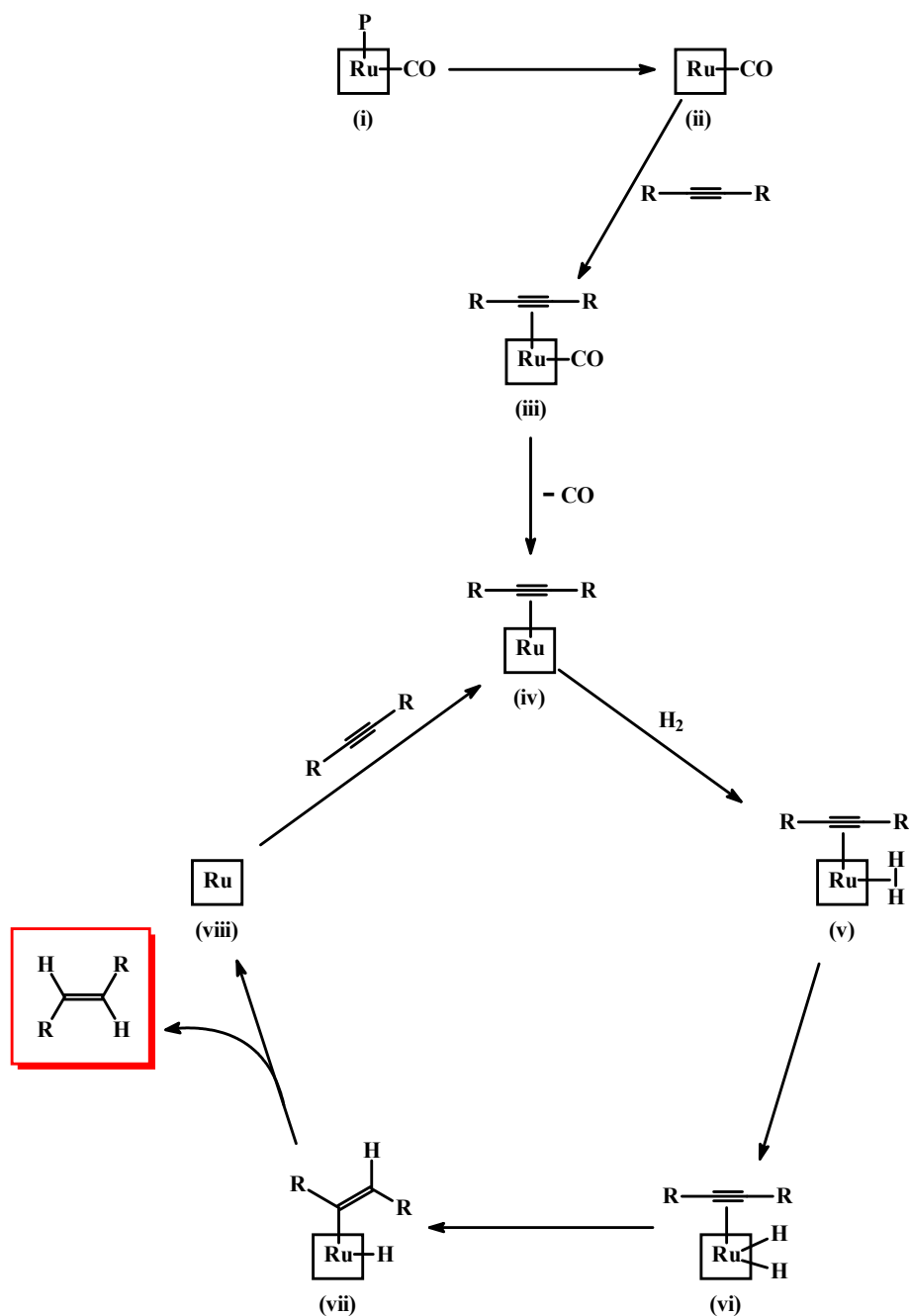
^c Determined by GCMS, for R₂ = H the product is indicated by P_n only.

^d Isolated yields are given within square brackets. For P_{8a} – P_{10b} isolated yields is calculated based on the ratio intensity of ¹H NMR signal of the two isomers.

4.2. Physical measurements

Microanalyses (C, H, N) were performed using a Heraeus Carlo Erba 1108 elemental analyzer. Mass spectra were recorded with a Micromass LCT electrospray (Qtof Micro YA263) mass spectrometer. NMR spectra were recorded in CDCl₃ solution on a Bruker Avance DPX 300 NMR spectrometer. IR spectra were obtained on a Perkin Elmer Spectrum Two IR spectrometer with samples prepared as KBr pellets. Electronic spectra were recorded on a JASCO V-

630 spectrophotometer. Magnetic susceptibilities were measured using a Sherwood MK-1 balance. Electrochemical measurements were made using a CH Instruments model 600A electrochemical analyzer. A platinum disc working electrode, a platinum wire auxiliary electrode and an aqueous saturated calomel reference electrode (SCE) were used in the cyclic voltammetry experiments. All electrochemical experiments were performed under a dinitrogen atmosphere. All electrochemical data were collected at 298 K and are uncorrected for junction potentials. Optimization of



Scheme 2. Probable mechanism for the observed hydrogenation of alkynes. In the pre-catalyst (i) only one ruthenium coordination environment is indicated, where P represents the coordinated phosphorus of a diphos ligand, and besides CO, no other coordinated ligands are shown.

ground-state structure, energy calculations, and molecular orbital calculations were carried out by density functional theory (DFT) method using the Gaussian 09 (B3LYP/GEN) package [31]. GC-MS analyses were performed using a Perkin Elmer CLARUS 680 instrument.

4.3. Syntheses of complexes

4.3.1. $[Ru_2(L^1)_3(CO)_2Cl_4]$, (**1**)

To a solution of $\{[Ru(CO)_2Cl_2]_n\}$ (50 mg, 0.22 mmol) in methanol (50 mL) 1,2-bis(diphenylphosphino)ethane (140 mg, 0.35 mmol) was added. The mixture was refluxed for 4 h, whereby complex **1** started precipitating as a light yellow solid, which was allowed to

settle by cooling the solution to room temperature. Then it was collected by filtration, washed thoroughly with diethyl ether and dried in air. Yield: 78%. Anal. Calcd. for $C_{80}H_{72}O_2P_6Cl_4Ru_2$: C, 60.21; H, 4.52. Found: C, 60.72; H, 4.49%. MS (ESI), positive mode: $[1 - Cl]^+$, 1558; $[1a - Cl]^+$, 960; $[1b - Cl]^+$, 562. 1H NMR [49]: 2.34–2.80 (12H) *; 6.97–7.60 (60H)*. ^{31}P NMR: 52.34 (t, $J_{P-H} = 36.3$); 50.36 (t, $J_{P-H} = 39.6$); 24.45 (t, $J_{P-H} = 39.7$). IR: 489, 512, 521, 562, 694, 740, 836, 878, 999, 1027, 1097, 1189, 1312, 1433, 1484, 1571, 1633, 1965, 2917 and 3054 cm^{-1} .

4.3.2. $[Ru_2(L^2)_3(CO)_2Cl_4]$, (**2**)

To a solution of $\{[Ru(CO)_2Cl_2]_n\}$ (50 mg, 0.22 mmol) in methanol (50 mL) 1,3-bis(diphenylphosphino)propane (140 mg, 0.34 mmol)

Table 6
Crystallographic data for complex **1**.

Empirical formula	C ₈₀ H ₇₂ O ₄ P ₄ Cl ₂ Ru ₂ ·2(C ₃ H ₆ O)
Formula weight	1711.29
Crystal system	monoclinic
Space group	P2 ₁ /n
a (Å)	12.8704(4)
b (Å)	11.2419(3)
c (Å)	27.5589(8)
β (°)	91.833(2)
V (Å ³)	3985.4(2)
Z	2
F(000)	1756
crystal size (mm)	0.14 × 0.16 × 0.24
T (K)	155
μ (mm ⁻¹)	0.684
Collected reflections	65033
R _{int}	0.068
Independent reflections	9170
R1 ^a	0.0489
wR2 ^b	0.1462
GOF ^c	0.96

^a R1 = $\sum ||F_o| - |F_c|| / \sum |F_o|$.

^b wR2 = $[\sum \{w(F_o^2 - F_c^2)\}^2 / \sum \{w(F_o^2)\}]^{1/2}$.

^c GOF = $[\sum \{w(F_o^2 - F_c^2)\}^2 / (M - N)]^{1/2}$, where M is the number of reflections and N is the number of parameters refined.

was added. The mixture was refluxed for 4 h, whereby a brown solution was obtained. The solvent was evaporated and the solid mass, thus obtained, was subjected to purification by thin-layer chromatography on a silica plate. With 1:2 acetonitrile-benzene as the eluant, a yellow band separated, which was extracted with acetonitrile. Evaporation of the acetonitrile extract gave complex **2** as a yellow solid. Yield: 44.5%. Anal. Calcd. for C₈₃H₇₈O₂P₆Cl₄Ru₂: C, 60.87; H, 4.77. Found: C, 60.35; H, 4.79%. MS (ESI), positive mode: [2 - Cl]⁺, 1600; [2a - Cl]⁺, 989; [2b - Cl]⁺, 577. ¹H NMR: 2.30–2.98 (18H)*; 6.66–8.14 (60H)*. ³¹P NMR: 20.51 (t, J_{P-H} = 37.1); 17.48 (t, J_{P-H} = 36.0); 8.60 (t, J_{P-H} = 38.8). IR: 500, 512, 518, 579, 698, 744, 838, 860, 999, 1027, 1094, 1189, 1315, 1434, 1483, 1638, 1961, 2924 and 3054 cm⁻¹.

4.3.3. [Ru₂(L³)₃(CO)₂Cl₄], (**3**)

This complex was synthesized by following the same procedure used for the synthesis of complex **1**, using 1,2-bis(diphenylphosphino)butane instead of 1,2-bis(diphenylphosphino)ethane. Yield: 81%. Anal. Calcd. for C₈₆H₈₄O₂P₆Cl₄Ru₂: C, 61.49; H, 5.01. Found: C, 61.44; H, 4.97%. MS (ESI), positive mode: [3 - Cl]⁺, 1642; [3a - Cl]⁺, 1017; [3b - Cl]⁺, 591. ¹H NMR: 2.27–2.92 (24H)*, 6.56–7.81 (60H)*. ³¹P NMR: 26.24 (t, J_{P-H} = 36.5); 25.61 (t, J_{P-H} = 37.4); 18.82 (t, J_{P-H} = 39.2). IR: 503, 514, 529, 576, 588, 696, 740, 833, 857, 1001, 1028, 1096, 1185, 1359, 1433, 1484, 1572, 1587, 1618, 1961, 2922 and 3052 cm⁻¹.

4.4. X-ray crystallography

Single crystals of complex **1** were obtained by slow evaporation of solvents from a solution of the complex in 1:3 dichloromethane-acetone. Selected crystal data and data collection parameters are given in Table 6. Data were collected on a Bruker SMART CCD diffractometer. X-ray data reduction, structure solution and refinement were done using the SHELXS-97 and SHELXL-97 packages [50]. The structure was solved by the direct methods.

4.5. General procedure for the alkyne hydrogenation

In a typical run, an oven-dried 10 mL two-neck round-bottomed

flask was charged with the phenylacetylene (0.5 mmol) and a known mol percent of the catalyst dissolved in toluene (5 mL). H₂-gas was passed through the solution continuously at 1 atm pressure. The flask was placed in a preheated oil bath at the required temperature. After the specified time, the flask was removed from the oil bath and the resultant solution was filtered through tight-packed slurry of silica (100–200 mesh) in hexane, and the filtrate was analyzed by GC-MS.

4.5.1. ¹H NMR of the product alkenes [49]

P₁: 5.27 (d, 1H, J = 10.9); 5.78 (d, 1H, J = 17.6); 6.75 (d of d, 1H, J = 17.5, 10.9); 7.25–7.46 (5H)*. **P**₂: 2.28 (s, 3H); 5.13 (d, 1H, J = 9.7); 5.67 (d, 1H, J = 17.0); 6.63 (d of d, 1H, J = 16.3, 9.9); 7.06–7.33 (4H)*. **P**₃: 3.72 (s, 3H); 5.06 (d, 1H, J = 11.0); 5.60 (d, 1H, J = 17.8); 6.68 (d of d, 1H, J = 17.2, 10.5); 6.80–7.21 (4H)*. **P**₄: 2.37 (s, 3H); 3.78 (s, 3H); 5.34 (d, 1H, J = 10.3); 5.44 (d, 1H, J = 16.9); 6.49–6.55 (2H)*; 6.90 (d of d, 1H, J = 16.2, 9.9); 7.21 (d, 1H, J = 7.5). **P**₅: 5.14 (d, 1H, J = 9.6); 5.62 (d, 1H, J = 16.4); 6.59 (d of d, 1H, J = 16.7, 9.7); 6.86–7.23 (4H)*. **P**₆: 5.21 (d, 1H, J = 9.8); 5.70 (d, 1H, J = 16.5); 6.66 (d of d, 1H, J = 16.8, 9.9); 7.18–7.42 (4H)*. **P**₇: 5.19 (d, 1H, J = 9.7); 5.68 (d, 1H, J = 16.5); 6.63 (d of d, 1H, J = 16.8, 9.8); 7.12–7.40 (4H)*. **P**_{8a} + **P**_{8b}: 1.73 (s)[#]; 1.81 (s); 5.95 (d, J = 10.2)[#]; 6.08 (d, J = 14.9); 6.22 (d, J = 10.9)[#]; 6.34 (d, J = 16.6); 6.91–7.39*. **P**_{9a} + **P**_{9b}: 6.66 (s)[#]; 7.02 (s); 7.09–7.51*. **P**_{10a} + **P**_{10b}: 6.94 (s)[#]; 7.17 (s); 7.05 (d, J = 6.5)[#]; 7.32 (d, J = 6.2); 8.23 (d, J = 7.8); 8.59 (d, J = 7.8).

Acknowledgments

The authors thank the reviewers for their constructive comments, which have been very helpful in preparing the revised manuscript. Financial assistance received from the Department of Science and Technology, Government of West Bengal, Kolkata [Sanction No. 746(Sanc./ST/P/S&T/2G-4/2013)], University Grants Commission, New Delhi [Sanction No. F.19-122/2014(BSR)] and Council of Scientific and Industrial Research, New Delhi [Grant No. 01(2788)/14/EMR-II] is gratefully acknowledged. The authors thank Dr. Saurabh Das (Department of Chemistry, Jadavpur University) for his help in recording the electronic spectra.

Appendix A. Supplementary data

Supplementary data related to this article can be found at <http://dx.doi.org/10.1016/j.jorganchem.2017.01.027>.

CCDC 1489485 contains the supplementary crystallographic data for this paper. DFT-optimized structure of complex **1** (Fig. S1), selected bond lengths (Å) and bond angles (°) for the DFT-optimized structures of complexes **1**, **2** and **3** (Table S1), probable alternative steps behind formation of the di-ruthenium complexes **1**–**3** (Scheme S1), DFT-optimized structures and ground-state energy ordering for the species shown in Scheme S1 (Fig. S2), and contour plots of the HOMO and LUMO of complexes **2** and **3** (Fig. S3 and Fig. S4) are available as supporting information.

References

- [1] Y. Nakamura, T. Ohta, Y. Oe, *Chem. Commun.* 51 (2015) 7459–7462.
- [2] S. Manzini, J.A. Fernández-Salas, S.P. Nolan, *Acc. Chem. Res.* 47 (2014) 3089–3101.
- [3] L. Ackermann, *Acc. Chem. Res.* 47 (2014) 281–295.
- [4] M.C. Warner, J.-E. Bäckvall, *Acc. Chem. Res.* 46 (2013) 2545–2555.
- [5] D.K. Dutta, B. Deb, *Coord. Chem. Rev.* 255 (2011) 1686–1712.
- [6] A.M. Lozano-Vila, S. Monsaert, A. Bajek, F. Verpoort, *Chem. Rev.* 110 (2010) 4865–4909.
- [7] G.C. Vougioukalakis, R.H. Grubbs, *Chem. Rev.* 110 (2010) 1746–1787.
- [8] B. Therrien, G.S. Fink, *Coord. Chem. Rev.* 253 (2009) 2639–2664.
- [9] S.E. Kabir, G. Hogarth, *Coord. Chem. Rev.* 253 (2009) 1285–1315.
- [10] R.D. Adams, B. Captain, *Acc. Chem. Res.* 42 (2009) 409–418.
- [11] A. Coleman, C. Brennan, J.G. Vos, M.T. Pryce, *Coord. Chem. Rev.* 252 (2008)

- 2585–2592.
- [12] J.-I. Ito, S. Ujiie, H. Nishiyama, *Chem. Commun.* (2008) 1923–1925.
- [13] R. Karvembu, R. Prabhakaran, K. Natarajan, *Coord. Chem. Rev.* 249 (2005) 911–918.
- [14] V. Conte, E. Elakkari, B. Floris, V. Mirruzzo, P. Tagliatesta, *Chem. Commun.* (2005) 1587–1588.
- [15] J.-P. Genet, *Acc. Chem. Res.* 36 (2003) 908–918.
- [16] R. Uma, C. Crévisy, R. Grée, *Chem. Rev.* 103 (2003) 27–52.
- [17] B.K. Dey, J. Dutta, M.G.B. Drew, S. Bhattacharya, *J. Organomet. Chem.* 750 (2014) 176–184.
- [18] J. Dutta, M.G. Richmond, S. Bhattacharya, *Eur. J. Inorg. Chem.* (2014) 4600–4610.
- [19] N. Saha Chowdhury, C. GuhaRoy, R.J. Butcher, S. Bhattacharya, *Inorg. Chim. Acta* 406 (2013) 20–26.
- [20] S. Datta, D.K. Seth, S. Halder, W.S. Sheldrick, H. Mayer-Figge, M.G.B. Drew, S. Bhattacharya, *RSC Adv.* 2 (2012) 5254–5264.
- [21] N. Saha Chowdhury, D.K. Seth, M.G.B. Drew, S. Bhattacharya, *Inorg. Chim. Acta* 372 (2011) 183–190.
- [22] E.R. dos Santos, M.A. Mondelli, L.V. Pozzi, R.S. Correa, H.S. Salistre-de Araujo, F.R. Pavan, C.Q.F. Leite, J. Ellena, V.R.S. Malta, S.P. Machado, A.A. Batista, *Olyhedron* 51 (2013) 292–297.
- [23] M. Webster, W. Zhang, *Inorg. Chem.* 49 (2010) 752–760.
- [24] C.D. Effendy, M. Nicola, C. Fianchini, B.W. Pettinari, N. Skelton, Somers A.H. White, *Inorg. Chim. Acta* 358 (2005) 763–795.
- [25] E. Fournier, S. Sicard, A. Decken, P.D. Harvey, *Inorg. Chem.* 43 (2004) 1491–1501.
- [26] S. Kundu, D. Sarkar, M.S. Jana, A.K. Pramanik, S. Jana, T.K. Mondal, *J. Mol. Struct.* 1035 (2013) 277–284.
- [27] B. Deb, P.P. Sarmah, D.K. Dutta, *Eur. J. Inorg. Chem.* (2010) 1710–1716.
- [28] P. Datta, S.K. Sarkar, T.K. Mondal, A.K. Patra, C. Sinha, *J. Organomet. Chem.* 694 (2009) 4124–4133.
- [29] B. Deb, B.J. Sarmah, B.J. Borah, D.K. Dutta, *Spectrochim. Acta Part A* 72 (2009) 339–342.
- [30] D. Oyama, A. Asuma, T. Hamada, T. Takase, *Inorg. Chim. Acta* 362 (2009) 2581–2588.
- [31] M.J. Frisch, G.W. Trucks, H.B. Schlegel, G.E. Scuseria, M.A. Robb, J.R. Cheeseman, G. Scalmani, V. Barone, B. Mennucci, G.A. Petersson, H. Nakatsuji, M. Caricato, X. Li, H.P. Hratchian, A.F. Izmaylov, J. Bloino, G. Zheng, J.L. Sonnenberg, M. Hada, M. Ehara, K. Toyota, R. Fukuda, J. Hasegawa, M. Ishida, T. Nakajima, Y. Honda, O. Kitao, H. Nakai, T. Vreven, J.A. Montgomery Jr., J.E. Peralta, F. Ogliaro, M. Bearpark, J.J. Heyd, E. Brothers, K.N. Kudin, V.N. Staroverov, R. Kobayashi, J. Normand, K. Raghavachari, A. Rendell, J.C. Burant, S.S. Iyengar, J. Tomasi, M. Cossi, N. Rega, J.M. Millam, M. Klene, J.E. Knox, J.B. Cross, V. Bakken, C. Adamo, J. Jaramillo, R. Gomperts, R.E. Stratmann, O. Yazyev, A.J. Austin, R. Cammi, C. Pomelli, J.W. Ochterski, R.L. Martin, K. Morokuma, V.G. Zakrzewski, G.A. Voth, P. Salvador, J.J. Dannenberg, S. Dapprich, A.D. Daniels, Ö. Farkas, J.B. Foresman, J.V. Ortiz, J. Cioslowski, D.J. Fox, *Gaussian 09, Revision E.01*, Gaussian, Inc., Wallingford CT, 2009.
- [32] E.R.T. Tiekink, *Z. Kristallogr.* NCS 216, 2001, pp. 69–70.
- [33] C.D. Effendy, M. Nicola, C. Fianchini, B.W. Pettinari, N. Skelton, Somers A.H. White, *Inorg. Chim. Acta* 358 (2005) 763–795.
- [34] A.V. Rivera, D. Gómez C, E. Rodulfo de Gil, T. Suárez, *Acta Cryst. C* 44 (1988) 277–279.
- [35] M. Al-Noaimi, I. Warad, O.S. Abdel-Rahman, F.F. Awwadi, S.F. Haddad, T.B. Hadda, *Polyhedron* 62 (2013) 110–119.
- [36] M. K. Karunananda, N. P. Mankad, DOI: <http://dx.doi.org/10.1021/acs.organomet.6b00356>.
- [37] K.T. Neumann, S. Klimczyk, M.N. Burhardt, B. Bang-Andersen, T. Skrydstrup, A.T. Lindhardt, *ACS Catal.* 6 (2016) 4710–4714.
- [38] M. Leutzsch, L.M. Wolf, P. Gupta, M. Fuchs, W. Thiel, C. Faras, A. Firstner, *Angew. Chem. Int. Ed.* 54 (2015) 12431–12436.
- [39] K. Radkowski, B. Sundararaju, A. Furstner, *Angew. Chem. Int. Ed.* 52 (2013) 355–360.
- [40] R.D. Adams, B. Captain, L. Zhu, *J. Organomet. Chem.* 691 (2006) 3122–3128.
- [41] P. Frediani, C. Giannelli, A. Salvini, S. Ianelli, *J. Organomet. Chem.* 667 (2003) 197–208.
- [42] Y. Shvo, I. Goldberg, D. Czerkic, D. Reshef, Z. Stein, *Organometallics* 16 (1997) 133–138.
- [43] R.D. Adams, T.S. Bamard, Z. Li, W. Wu, J.H. Yamamoto, *J. Am. Chem. Soc.* 116 (1994) 9103–9113.
- [44] M.C. MacInnis, R. McDonald, M.J. Ferguson, S. Tobisch, L. Turculet, *J. Am. Chem. Soc.* 133 (2011) 13622–13633.
- [45] J.P. Lee, Z. Ke, M.A. Ramirez, T.B. Gunnoe, T.R. Cundari, P.D. Boyle, J.L. Petersen, *Organometallics* 28 (2009) 1758–1775.
- [46] A. Walstrom, M. Pink, K.G. Caulton, *Inorg. Chem.* 45 (2006) 5617–5620.
- [47] L.A. Watson, O.V. Ozerov, M. Pink, K.G. Caulton, *J. Am. Chem. Soc.* 125 (2003) 8426–8427.
- [48] P.A. Anderson, G.B. Deacon, K.H. Haarmann, F.R. Keene, T.J. Meyer, D.A. Reitsma, B.W. Skelton, G.F. Strouse, N.C. Thomas, J.A. Treadway, A.H. White, *Inorg. Chem.* 34 (1995) 6145–6157.
- [49] Chemical shifts for all NMR data are given in ppm and the multiplicity of the signals, along with the associated coupling constant(s), is given in parentheses. Overlapping signals are marked with an asterisk (*). In the NMR data of the mixture of two isomeric products obtained from catalysis, hash (#) represents signals with much less intensity.
- [50] G.M. Sheldrick, *SHELXS-97 and SHELXL-97, Fortran Programs for Crystal Structure Solution and Refinement*, University of Gottingen, Gottingen, Germany, 1997.